

Cite this: *Dalton Trans.*, 2012, **41**, 777

www.rsc.org/dalton

PAPER

Mechanistic investigation of cyclohexane oxidation by a non-heme iron complex: evidence of product inhibition by UV/vis stopped-flow studies†

Lauren C. Gregor,^a Gerard T. Rowe,^a Elena Rybak-Akimova^b and John P. Caradonna^{*a}

Received 28th September 2011, Accepted 1st October 2011

DOI: 10.1039/c1dt11841b

We report herein studies examining a binuclear non-heme iron model complex that is capable of catalytically oxidizing cyclohexane to cyclohexanol in excess of 200 turnovers, relative to the iron complex, and cyclohexanone (5 turnovers) *via* heterolytic cleavage of the mechanistic probe peroxide MPPH. Low-temperature stopped-flow electronic spectroscopy was utilized to investigate the mechanism of the reaction of this diiron(II) compound, $\text{Fe}_2(\text{H}_2\text{Hbamb})_2(\text{N-MeIm})_2$, ($\text{H}_2\text{Hbamb} = 2,3\text{-bis}(2\text{-hydroxybenzamido})\text{dimethylbutane}$) (**1**) with MPPH. In the absence of substrates, the reaction proceeds in three consecutive steps starting with oxygen atom transfer to the diferrous complex to generate a putative $[\text{Fe}^{\text{IV}}=\text{O}]$ species, thought to be the oxidant in the catalytic cycle. Over time, the rate of catalysis is observed to decrease without consumption of all available peroxide. By utilizing low-temperature stopped-flow UV/vis kinetic studies, the diferrous complex, **1**, is shown to undergo product inhibition arising from the interaction of either cyclohexanol or MPP-OL product species to the diiron center, therefore precluding further reaction with MPPH.

Introduction

Binuclear non-heme iron(II) monooxygenases represent a subset of carboxylate-bridged diiron enzymes that utilize O_2 during the conversion of C–H to C–OH bonds of thermodynamically challenging substrates with the concomitant formation of H_2O .¹ Well defined members of this subset include soluble methane monooxygenase (sMMO), which oxidizes methane to methanol at ambient temperatures and pressures,^{2–5} toluene monooxygenase (TOMO)^{6,7} and phenol hydroxylase.⁸ Each of these enzymes is thought to proceed *via* a high-valent iron intermediate ($[\text{Fe}^{\text{III}}, \text{Fe}^{\text{V}}=\text{O}] \leftrightarrow [\text{Fe}^{\text{IV}}, \text{Fe}^{\text{IV}}=\text{O}]$; $[\text{Fe}^{\text{IV}}(\mu\text{-O})_2\text{Fe}^{\text{IV}}]$) that is capable of oxidizing the particular cognate substrate.^{9–12} In depth UV/vis stopped-flow kinetic studies on sMMO show the presence of a kinetically competent reactive intermediate, compound **Q**,^{13–15} that is currently assigned as a diferryl-di- μ -oxo species ($[\text{Fe}^{\text{IV}}(\mu\text{-O})_2\text{Fe}^{\text{IV}}]$)^{13,15,16} based on rapid-freeze quench spectroscopic studies.^{14–16}

We have examined a series of binuclear non-heme iron oxygenase model compounds based on diamide ligands¹⁷ that utilize an oxygen-rich coordination environment (Fig. 1) about the iron centers.^{18–22} The binuclear iron(II) complexes have been structurally characterized and each iron center shown to have an NO_4 ligand environment resulting in a trigonal-bipyramidal coordination

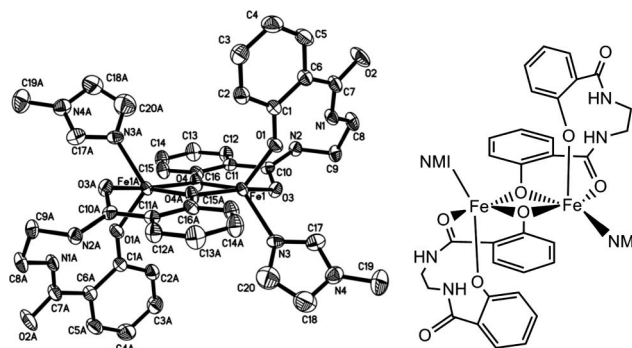


Fig. 1 Crystal structure of $[\text{Fe}^{\text{II}}\text{Fe}^{\text{II}}(\text{H}_2\text{Hbame})_2(\text{NMI})_2]$, **1**.²¹

with amide oxygen atoms, terminal and bridging phenolates, and a nitrogen from *N*-methylimidazole (Fig. 1).²² Fig. 1 shows the crystal structure of the closely related binuclear iron(II) complex $[\text{Fe}_2(\text{H}_2\text{Hbame})_2(\text{N-MeIm})_2]$ (**1**; *N-MeIm* = *N*-methylimidazole; $\text{H}_2\text{Hbamb} = 2,3\text{-bis}(2\text{-hydroxybenzamido})\text{dimethylbutane}$).

Experimental

General experimental procedures

1^{S1} and MPPH^{S2–4} were synthesized according to previously published procedures. The peroxide content of MPPH was determined to be >98% by iodometric titration.^{S5} Metal ion impurities were excluded from all glassware involved in peroxide synthesis and handling by soaking in a solution of aqueous EDTA (50 mM) for at least 12 h prior to use. 2-Methyl-1-phenylprop-2-yl alcohol

^aDepartment of Chemistry, Boston University, Boston, Massachusetts, 02215, USA

^bDepartment of Chemistry, Tufts University, Medford, Massachusetts, 02115, USA

† Electronic supplementary information (ESI) available. See DOI: 10.1039/c1dt11841b

(98%) and magnesium turnings were obtained from Sigma-Aldrich. Hexachloroacetone (99%+) and benzyl chloride (ACS) were obtained from Acros Organics. Hydrogen peroxide (70%, tech grade) was donated to the lab by the FMC corporation. Prior to use, dimethylformamide (Pharmco, HPLC grade) was processed through a PureSolv solvent purification system from Innovative Technologies. The dimethylformamide from the solvent purification system was also distilled over phosphorus pentoxide (Acros Organics, ACS grade). Unstabilized dichloromethane was obtained from Fisher and was distilled over calcium hydride before use. All of the solvents used in air-sensitive work were thoroughly degassed by subjecting them to at least six successive freeze-pump-thaw cycles, after which they were transferred to an inert atmosphere glove box, in which all of the solution preparations were carried out. Cyclohexanol and 2-methyl-1-phenylprop-2-yl alcohol (MPP-OL) were distilled over sodium, methanol was distilled over magnesium metal, and each alcohol was degassed and freeze-pump-thawed prior to use.

Stopped-flow spectroscopy and data analysis

Single-mixing stopped-flow spectroscopy was performed at Tufts University on a Hi-Tech Scientific SF-43 cryogenic double-mixing stopped-flow system operating in single-mixing mode. Low temperatures were maintained through the use of a liquid-nitrogen-cooled heptane bath equipped with a cryostat. To maintain an anaerobic environment, all of the solutions were prepared in an inert atmosphere box and transferred into the stopped-flow spectrometer using gastight syringes. Hi-Tech Scientific IS-2 Rapid Kinetics software package was used to control the instrument and collect data. For each single-wavelength data set, 512 samples were collected in a linear time base. Fits of kinetic data to appropriate models were performed using non-linear least-squares fitting methods contained in Specfit/32 version 3.0.36. Time-resolved spectra were acquired with TgK Scientific (formerly HiTech Scientific, Salisbury, Wiltshire, UK) SF-61DX2 cryogenic Stopped-flow system equipped with J&M Diode array (Spectralytics).

Synthesis of 2-benzyl-1,1,1,3,3,3-hexachloropropan-2-ol (MPP-OL-Cl₆)

A sealed round bottomed flask equipped with a condenser and an oil bubbler was charged with magnesium turnings (1.9 g, 78 mmol), dry diethyl ether (250 mL) and a magnetic stir bar. To this flask, benzyl chloride (10 g, 9.1 mL, 79 mmol) was added *via* syringe. The solution was refluxed for a half hour until the magnesium metal was consumed and a blackish blue solution formed. This solution was cooled on an ice bath, and hexachloroacetone (21 g, 12 mL, 79 mmol) was slowly added over the course of 20 min, during which time a precipitate formed. When the addition was complete, the solution was warmed to room temperature and refluxed for 2 h before quenching with water, followed by the addition of 0.5 M HCl to make sure the precipitate dissolved. The mixture was extracted three times with 100 mL diethylether. The organic layers were combined and dried with magnesium sulfate. Solvent was removed by rotary evaporation, leaving an oil which was purified by vacuum distillation, discarding the initial fraction of hexachloroacetone to yield a yellow crystalline solid. Yield: 4.1

g (14%) ¹H-NMR δ (CDCl₃): 2.927 (s, 2.0), 7.216 (m, 2.81), 7.290 ppm (d, 1.90); ¹³C-NMR δ (CDCl₃): 38.09, 126.06, 128.47, 128.59, 141.92 ppm.

Synthesis of 1-benzyl-2,2,2-trichloro-1-(trichloromethyl)ethyl hydroperoxide (MPPH-Cl₆)

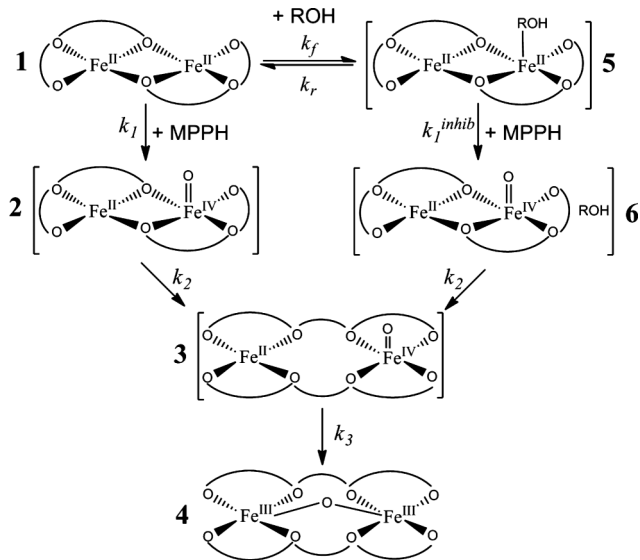
A solution of MMP-OL-Cl₆ (4 g, 11 mmol) in hexane (25 mL) was added to a flat bottomed boiling flask equipped with a cross-shaped stir bar, and stirred vigorously. The solution was heated to 40 °C in an oil bath and carefully maintained at that temperature during the course of the reaction. 70% H₂O₂ (50 mL, 1.1 mmol) and sulfuric acid (1 mL) were thoroughly mixed in an addition funnel. The acid-peroxide solution was slowly dripped into the solution of alcohol. When addition was complete, the reaction was stirred at 40 °C for 22 h. The reaction vessel was cooled and water immediately added to dilute unreacted hydrogen peroxide. The organic layer was removed, and the aqueous layer extracted three times with 15 mL portions of hexane. The organic phases were combined and dried with magnesium sulfate before removal of solvent with a stream of N₂ gas. A slightly oily crystalline solid was obtained that was recrystallized from warm hexane to yield the product. Iodometric titration of the solid confirmed 97% peroxide activity. Product is stored at -40 °C until needed. Yield: 2.5 g (60%) ¹H-NMR δ (CDCl₃): 2.923 (s, 2.0), 7.194 (m, 3.0), 7.283 ppm (m, 1.8); ¹³C-NMR δ (CDCl₃): 39.10, 124.80, 127.16, 127.27, 140.26 ppm.

Results and discussion

We previously reported the ability of **1** to catalytically oxidize cyclohexane²³ to cyclohexanol in excess of 200 turnovers (relative to **1**) and subsequently 5 turnovers of cyclohexanone (relative to **1**) through heterolytic cleavage of the O–O bond of the mechanistic probe peroxide, 2-methyl-1-phenylprop-2-yl hydroperoxide (MPPH).²⁰ It was noticed, however, that the rate of product formation appeared to decrease as a function of time prior to full consumption of either MPPH or cyclohexane (ESI, Fig. S9†).²³ The loss of catalytic activity was not due to catalyst inactivation to the inert μ -oxo diiron(III) complex, **4**, as **4** produces only homolytic cleavage products of MPPH (ESI, Fig. S8†) while only heterolytic cleavage products were observed by GC-MS studies during catalysis.²³ We present herein evidence for product inhibition by utilizing anaerobic low-temperature UV/vis stopped-flow kinetic methods.

Detailed investigation of the interaction of **1** with MPPH^{20,21} indicated that the diferrous compound induces heterolytic O–O bond cleavage (ESI Fig. S8†) as determined by GC-MS analyses of the resulting product distributions in which MPP-OL was observed as the sole product. Furthermore, temperature dependent kinetic studies showed, in the absence of substrate, that the reaction of **1** with MPPH,²⁰ or oxygen atom donor molecules,²¹ proceeds *via* a three step process, currently assigned as an oxygen-atom transfer to a ferrous center to form a high-valent intermediate **2** (*k*₁ step), ligand rearrangement of the metal complex to form **3** (*k*₂ step),²² followed by decay to the diferric μ -oxo compound **4** (*k*₃ step) (Scheme 1).^{20,21}

The temperature dependence of the *k*₁ process was determined (Table 1) and gave an entropy of activation that is significantly



Scheme 1 Proposed mechanism of the reaction of **1** with alcohols and MPPH at $-80\text{ }^\circ\text{C}$ (193 K).

Table 1 Activation parameters for k_1 step with different oxidants

Oxidant	$k_{1(188\text{K})}$ ($\text{s}^{-1}\text{M}^{-1}$)	ΔH^\ddagger (kJ mol^{-1})	ΔS^\ddagger ($\text{J mol}^{-1}\text{K}^{-1}$)
MPPH	10(1)	30(4)	-60(18)
<i>p</i> -CN-DMANO	4.7×10^3	36(4)	21(18)

more negative than that measured for the oxygen atom donor molecules, *p*-CN-DMANO (Table 1).²¹

In comparison to the reaction of **1** with OAD molecules, the initial k_1 reaction of **1** with MPPH is slower at low temperatures. The peroxide exhibits rates that are seven to 400 times slower than 2,6-dimethyldiosylbenzene and 4-(dimethyl-amino)benzoxirone N-oxide, respectively.²¹ This resulted in similar activation enthalpies for both the peroxide (ΔH^\ddagger 30(4) kJ mol^{-1}) and the N-oxide (ΔH^\ddagger 36(4) kJ mol^{-1}), despite very different values for k_1 . These data indicate that k_1 may not depend solely on cleavage of the X–O bond. Rather, the k_1 values seem to exhibit a strong dependence on the entropy of activation, a result that is expected for a two-step mechanism with a requisite rapid (but left-lying) pre-equilibrium peroxide binding step (Scheme 2).²⁰



Scheme 2 Proposed mechanism for the initial interaction of **1** with MPPH.

The sign and magnitude of the entropy of activation represents the degree to which oxidant binding plays a role in determining the rate of the reaction. A large negative entropy of activation would be expected for a process of two molecules coming together. A larger positive entropic effect would be expected for a more dissociative process. However, it is currently unclear whether oxidant binding or X–O bond cleavage is the dominant factor and further studies are currently underway.

To further probe the bond cleavage process, we examined the influence of electron withdrawing substituents on the rate of heterolytic peroxide O–O bond cleavage. Previous studies demonstrated that peroxides and peracids with lower $\text{p}K_a$ values

react with metal porphyrins systems at a greater rate than their more basic counterparts.^{24,25} It was hypothesized that the transition state representing the heterolytic O–O bond cleavage process exhibits partial anionic character at the oxygen atom distal to the metal center (Fig. 2), suggesting that the presence of electron withdrawing groups on the methyl arms on the quaternary carbon of MPPH should help stabilize the negative charge generated during the O–O bond breaking step.

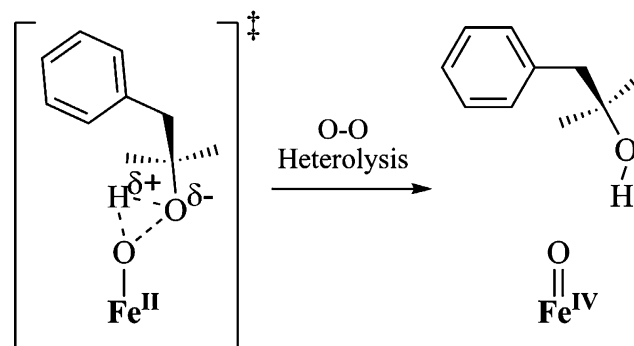


Fig. 2 Proposed transition state formed in the process of O–O bond heterolysis of a metal-bound peroxide species.

In order to probe the dependency between the rate of O–O bond cleavage and the stability of the alkoxide product produced *via* O–O heterolysis, a highly electron withdrawing derivative of MPPH, MPPH-Cl₆, was designed and synthesized containing two trichloromethyl groups in place of the methyl substituents present in MPPH. MPPH-Cl₆ reacts with **1** to produce an iron-based intermediate with an equivalent chromophore to that observed with MPPH or OAD molecules, consistent with O–O bond heterolysis and oxygen atom transfer to the ferrous site.^{20,21} Analysis of the kinetic data collected in single wavelength mode at 438 nm at $-75\text{ }^\circ\text{C}$ (198 K), is consistent with a three step process analogous to that reported for the reaction of **1** with either MPPH or OAD molecules. Consequently, the kinetic data for MPPH-Cl₆ with MPPH was fit to the same model (Fit to equations S6, S7, S9–11, S13 in the ESI†). These data indicate that the k_1 process for MPPH-Cl₆ ($235\text{ M}^{-1}\text{ s}^{-1}$) is 10 times greater than that determined for MPPH ($22\text{ M}^{-1}\text{ s}^{-1}$) (ESI Fig. S7†), consistent with interpretations that the enhanced electron withdrawing properties of MPPH-Cl₆ help to stabilize the negative charge buildup required for heterolytic cleavage of the O–O bond of the peroxide and therefore enhance the O–O bond cleavage reaction rate.

Efforts were then directed towards understanding potential sources of apparent catalyst inhibition. Alcohols are known to be weakly coordinating ligands to metal centers as neutral donor ligands²⁶ and are reported to inhibit catalysis with vanadium and molybdenum complexes.^{27,28} The catalytic reaction of **1** and MPPH with cyclohexane as substrate gives rise to alcohol products that could potentially bind to the diiron complex and influence catalysis. In addition to the generation of the cyclohexanol product at the iron center, the heterolytic cleavage of MPPH also results in the formation of 2-methyl-1-phenylprop-2-ol (MPP-OL), either of which could serve as inhibitors. Consequently, a series of kinetic experiments were designed to examine the reaction of **1** with MPPH in the presence of increasing alcohol concentrations in order to investigate the influence of this potential inhibitor on

the three processes (k_1 , k_2 , and k_3 steps) shown in Scheme 1. The oxidation of cyclohexanol was not included in any kinetic models, as the conversion of cyclohexanol to cyclohexanone is slow (250 min) compared to the single-turnover stopped-flow time scale (<500 s).^{20,23} Varying amounts (100, 500, 1000 equivalents) of deoxygenated alcohol (cyclohexanol, MPP-OL, CH₃OH) were added to anaerobic solutions of **1** (final concentration 0.08 mM, 70:30 DCM:DMF, (v/v)) and then reacted under pseudo-first order conditions with MPPH (9.2 mM) at -80 °C (193 K). These data, obtained by single-mixing stopped-flow UV/vis spectroscopy, were then analyzed at 438 nm (chromophore of **2**, $\epsilon \sim 3000 \text{ M}^{-1} \text{ cm}^{-1}$) and ultimately fit to the kinetic model shown in Scheme 1 (kinetic data fit to equations S1–S13, ESI†).

The best-fit mechanism requires a pre-equilibrium first step where **1** forms an adduct complex, **5**, in which the alcohol moiety is presumably coordinated to or interacts with the diiron centers. Data simulations suggest that the adduct complex **5** then reacts with MPPH (k_1^{inhib}) at a significantly reduced rate than with **1** (k_1 , Table 2). Previous mechanistic studies assigned the second step in the mechanism as a phenolate/amide carbonyl shift (PAC-shift),^{20–22} a ligand reorganization that is observed for both **2** and **6** and whose rate appears to be independent of the presence of alcohol. Crystallographic characterization of a series of [Fe^{II},Fe^{II}]/[Fe^{III}/Fe^{III}] compounds within the same ligand family (Fig. 1), which differ only in the amide linkage on the backbone of the ligand (*o*-phenylenediamine, 1,2-diaminocyclohexane, and ethylene diamine) confirmed the presence of a ligand rearrangement upon oxidation of the [Fe^{II},Fe^{II}] compounds (Fig. 3).²²

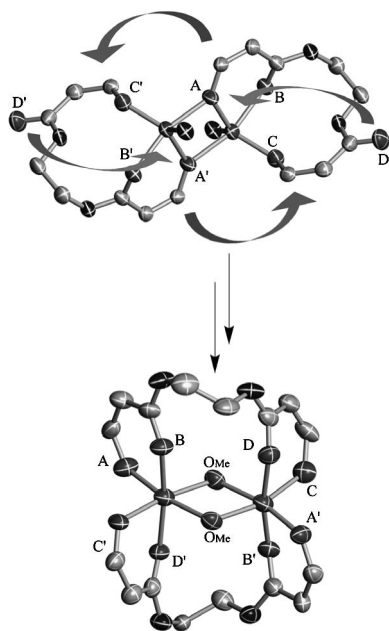


Fig. 3 Depiction of the ligand binding mode changes that occur upon oxidation. Some atoms omitted for clarity.²²

Upon oxidation, several structural changes occur (i) the loss of the *N*-MeIm ligands on each metal center (Fig. 1), (ii) the replacement of the two bridging phenolates with two bridging methoxy groups (crystal growth from methanol solutions), and (iii) the change in geometry about each iron center from five-coordinate trigonal bipyramidal to six-coordinate octahedral

(Fig. 3).²² This observed PAC-shift can be compared to the carboxylate shift observed in binuclear non-heme iron enzymes such as sMMO where the monodentate $\mu\text{-}\eta^1, \eta^2$ carboxylate bridged oxygen atom shifts away from the diiron core when oxidized to convert to a non-coordinating ligand.^{2,22}

Finally, the collapse of the rearranged intermediate to the μ -oxo ferric dimer end product is observed, which was confirmed by independent synthesis and NMR characterization of **4**.^{20,21} The value for k_1 was fixed to the rate previously determined²⁰ in each kinetic model examined to reduce the number of fitting parameters. The final model was able to predict values for k_2 and k_3 which compare favorably to those previously determined for the reaction of **1** with MPPH in the absence of added alcohol, reinforcing the proposed kinetic model.²⁰

Multiple mechanistic models were considered but eliminated due to poor fits to the time-dependent kinetic data. Among the models considered were simple pathways such as three sequential steps ($k_1 \rightarrow k_2 \rightarrow k_3$) similar to the proposed mechanism of **1** with MPPH in the absence of alcohol (Scheme 1) as well as the inclusion of an additional step to account for the addition of alcohol ($k_1 \rightarrow k_2 \rightarrow k_3 \rightarrow k_4$). Each of these scenarios resulted in poor kinetic fits (ESI Fig. S16, S17†) and unacceptable approximations for the known rates previously determined for the k_2 and k_3 processes. An additional more complex model excluded a pre-equilibrium step but assumed that the alcohol, once coordinated to the iron centers, does not readily dissociate. In this model, both the starting complex **1** and adduct complex **5** were assumed capable of reacting with MPPH. Simulations based on this model, however, also resulted in unacceptable kinetic fits (ESI Fig. S18†), suggesting the necessity to include an alcohol dissociation (k_r) step. Finally, a model including an alcohol equilibrium binding step but limiting the MPPH cleavage reaction to only compound **1** (not adduct **5**, *i.e.*, no k_1^{inhib} step) gave rise to poor fits (ESI Fig. S19†) of the time dependent data and unacceptable approximations of the known k_2 and k_3 rates, again suggesting the inclusion of the k_1^{inhib} process as an available pathway in any proposed mechanism. In each attempted model without including a pre-equilibrium step, the poor fit (large residuals to the fit) was observed in the early time points of the reaction (ESI Fig. S16–S18†), further suggesting that the pre-equilibrium step was required in the model.

Single-wavelength data (438 nm) and simulations for the reaction of **1** with MPPH and 100 equivalents of cyclohexanol are shown in Fig. 4. The inset shows the single wavelength data of **1** with MPPH in absence of cyclohexanol (—) followed by additional equivalents of cyclohexanol. There is a clear and observable decrease in the slope of the initial rate process (first 10 s) with increasing equivalents of pre-incubated cyclohexanol.

These concentration-dependent data are consistent with the presence of a pre-equilibrium process and show a clear effect on the initial rate of the reaction of **1** with MPPH; in the presence of cyclohexanol, the overall set of reactions takes longer to reach the final absorbance characteristic of complete μ -oxo dimer, **4**, formation. The decrease in observed absorbance is not due to dilution of **1** by the addition of alcohol as an identical concentration of **1** was maintained throughout all experiments.

The proposed mechanism was further challenged by examining the effect of CH₃OH and MPP-OL (Table 2) as inhibitors owing to their greater expected tendencies to coordinate to metal centers. Interestingly, the addition of 1 equivalent of the tight

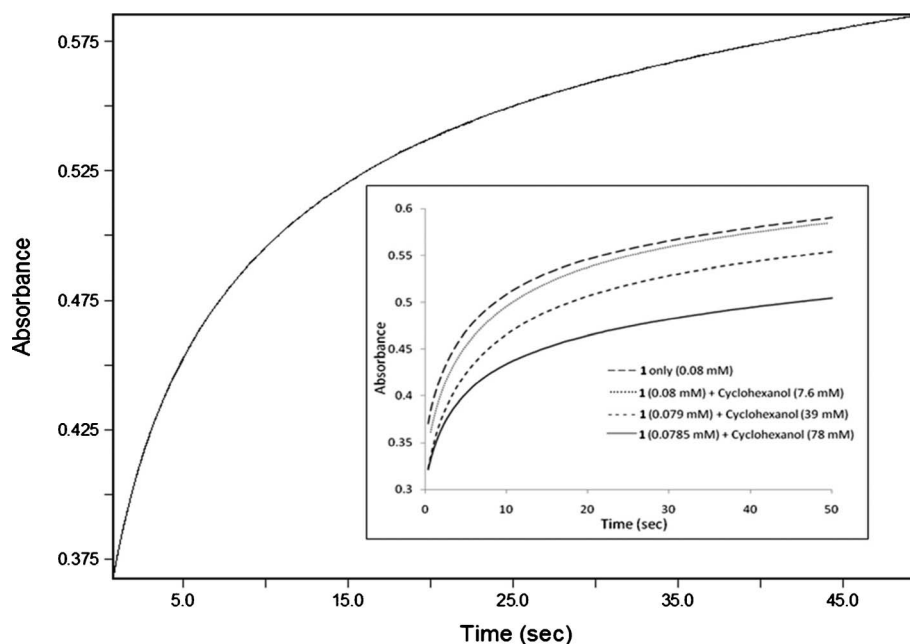


Fig. 4 Single wavelength data and kinetic fit for **1** (0.08 mM) and MPPH (9.2 mM) with cyclohexanol (7.6 mM). Inset: Effect of single-wavelength data by addition of cyclohexanol.

Table 2 Kinetic data fit to the model described in Scheme 1

X-OH	K_{eq} (k_f/k_r)	k_1 ($\text{M}^{-1} \text{s}^{-1}$)	k_1^{inhib} ($\text{M}^{-1} \text{s}^{-1}$)	k_2 (s^{-1})	k_3 (s^{-1})
No alcohol	—	14(1)	—	0.12(2)	0.007(1)
Cyclohexanol	127 ± 40	17(2)	$9.3(4) \times 10^{-6}$	0.12(2)	0.006(1)
MPP-OL	230 ± 30	16(3)	0.02(3)	0.13(1)	0.005(2)
CH_3OH	716 ± 20	16(2)	0.008(3)	0.13(1)	0.006(1)

binding ligand hydroxyurea was sufficient to completely inhibit the reaction of **1** (0.19 mM) with oxygen atom donor molecules at -75°C (ESI, Fig. S13†).

Simulation of the kinetic data using the model depicted in Scheme 1 allows insights into the initial rapid equilibrium (K_{eq} , k_f/k_r) step for each alcohol (Table 2). The K_{eq} values in Table 2 represent an average of the K_{eq} values calculated for 100, 500, and 1000 equivalents of each alcohol; the K_{eq} values determined for the different concentrations of alcohol were comparable within standard error (ESI, Tables S1–S3†).

The data in Table 2 parallels the relationship between the K_{eq} values and the relative ability of the alcohols to coordinate to the iron center. It is of further interest that the determined k_2 , and k_3 rates are independent of the nature of the alcohol and that these values are comparable to the rates of **1** and MPPH obtained in the absence of any added alcohol. These observations suggest that the presence of alcohol has little or no discernable effect on the multi-step reaction of **1** with MPPH other than to act as an initial inhibitor. The rates for k_1^{inhib} (the adduct complex **5** reacting with MPPH) are significantly slower than the rates for k_2 , suggesting very little overall contribution from the k_1^{inhib} pathway (only a small amount of **5** reacts with MPPH to contribute to the kinetic model). The absence of a k_1^{inhib} in the kinetic model, though, does result in poor residuals for the kinetic fits, suggesting that a k_1^{inhib} step is operational.

Additional experiments indicated evidence of adduct formation between **1** and alcohols. Electrochemical studies were performed in the presence and absence of cyclohexanol to probe the possible electronic effects of coordinated alcohol on the diiron center. Cyclic voltammetry studies utilizing a glassy carbon electrode were consistent with previously published results^{18,19} and show the presence of two quasi-reversible one-electron oxidation steps at -690 mV and -310 mV vs. NHE corresponding to $[\text{Fe}^{\text{II}}, \text{Fe}^{\text{II}}] \rightarrow [\text{Fe}^{\text{II}}, \text{Fe}^{\text{III}}]$ and $[\text{Fe}^{\text{II}}, \text{Fe}^{\text{II}}] \rightarrow [\text{Fe}^{\text{III}}, \text{Fe}^{\text{III}}]$ core oxidations. The addition of cyclohexanol (310, 600, and 870 mM) in the electrochemical cell at constant concentration of **1** showed a concentration-dependent decrease in the intensity of the $[\text{Fe}^{\text{II}}, \text{Fe}^{\text{II}}] \rightarrow [\text{Fe}^{\text{II}}, \text{Fe}^{\text{III}}]$ couple versus the $[\text{Fe}^{\text{II}}, \text{Fe}^{\text{II}}] \rightarrow [\text{Fe}^{\text{III}}, \text{Fe}^{\text{III}}]$ couple, suggesting that the cyclohexanol is either affecting the binding of **1** to the electrode surface or influencing the ability of **1** to be oxidized.

Additional control reactions excluded any significant deleterious effect of cyclohexanol on the oxidant, MPPH. The oxidation of triphenylphosphine (PPh_3) to triphenylphosphine oxide ($\text{O}=\text{PPh}_3$) in the absence of catalyst was used as a surrogate reaction to examine if the presence of cyclohexanol has any effect on the ability of MPPH to oxidize organic substrates. Reactions of MPPH (3.9 mM) and PPh_3 (27.5 mM) in 70 : 30 DCM : DMF (v/v), performed in the absence and presence of cyclohexanol (480 mM), gave equivalent quantities of $\text{O}=\text{PPh}_3$ product by GC-MS analysis, indicating that cyclohexanol has no discernable

influence on the thermodynamic stability of MPPH or its intrinsic reactivity towards PPh₃.

In this paper, we report kinetic evidence that a binuclear non-heme iron model complex capable of catalytically oxidizing cyclohexane to cyclohexanol suffers from product inhibition. It is therefore interesting to compare our synthetic model chemistry to metalloenzyme systems in order to highlight differences between homogeneous small molecule catalysts and enzyme active site metal chemistry that is internally sequestered and environmentally regulated by the protein matrix. Binuclear non-heme iron enzymes, such as soluble methane monooxygenase (sMMO) or toluene monooxygenase (TOMO), are designed and have evolved such that they do not suffer from product inhibition under normal conditions. sMMO possess a very broad substrate specificity and is capable of catalyzing both oxidation and epoxidation reactions, depending on the substrate.²⁹ In the case of sMMO, the apparent K_m for methanol (0.95 mM) and methane (0.16 mM) have been established suggesting that methanol has a relatively poor affinity for the enzyme,²⁹ consistent with the observed lack of product inhibition. Crystallography studies of both sMMO³⁰ and TOMO³¹ have shown evidence for substrate channels and cavities within the protein structure. In the case of sMMO, two channels with significant hydrophobic character were identified and proposed to facilitate methane and dioxygen transport into the active site. However, crystals grown in the presence of methanol found no methanol molecules present in these cavities.³⁰ These data suggest that there might be a different pathway for methanol to leave the active site³⁰ in order to efficiently transport substrate and product during catalysis. TOMO was also found to have a single channel large enough to accommodate aromatic substrates or products to or from the active site.³¹ This channel was found to contain both hydrophobic and hydrophilic residues suggesting it may facilitate both entrance and exit to the active site.³¹

Enzymes have been shown to be affected by product inhibition. One in particular is from the related family of mononuclear non-heme iron enzymes, tyrosine hydroxylase (TyrH).^{10,32,33} TyrH catalyzes the conversion of tyrosine to L-DOPA and has been shown to be affected by product inhibition. The product, L-DOPA is a catechol which once synthesized by the enzyme can coordinate to the iron center in the active site.³⁴

The chemistry of model complexes is performed in homogeneous solution with little control over what happens to the product once it is formed. Unlike an enzyme, which may contain substrate channels and may undergo global structural changes designed to release product from the active site after the reaction is completed,³⁵ small molecule analogs are more susceptible to product inhibition as reactions proceed. One way to overcome the issue of product inhibition is to develop continuous flow catalysis methods where there is a constant flow of substrate over the catalyst which results in product being washed away after the reaction is completed.³⁶ Such efforts are currently underway.

Conclusions

We present low-temperature stopped-flow kinetic evidence for product inhibition in the oxidation of cyclohexane to cyclohexanol during the reaction of diferrous complex **1** with MPPH. A proposed mechanism, consistent with the observed data, contains a pre-equilibrium step where the alcohol coordinates to the metal

center and inhibits the reaction of diferrous **1** with the oxidant MPPH. We also observe a clear dependence of the K_{eq} value on the nature of the corresponding alcohol. The results presented here suggest an explanation for the depletion of the catalytic activity observed during the oxidation of cyclohexane and indicate the sensitivity of this catalyst towards Lewis bases.

References

- 1 E. Y. Tshuva and S. J. Lippard, *Chem. Rev.*, 2004, **104**, 987–1011.
- 2 M. H. Baik, M. Newcomb, R. A. Friesner and S. J. Lippard, *Chem. Rev.*, 2003, **103**, 2385–2419.
- 3 B. J. Wallar and J. D. Lipscomb, *Chem. Rev.*, 1996, **96**, 2625–2657.
- 4 H. Dalton, *Advanced Applications of Microbiology*, 1980, **48**, 371–399.
- 5 H. Dalton, P. C. Wilkins and Y. Jiang, *Biochem. Soc. Trans.*, 1993, **21**, 749–752.
- 6 G. M. Whited and D. T. Gibson, *J. Bacteriol.*, 1991, **173**, 3010–3016.
- 7 L. M. Newman and L. P. Wackett, *Biochemistry*, 1995, **34**, 14066–14076.
- 8 N. Mitić, S. J. Smith, A. Neves, L. W. Guddat, L. R. Gahan and G. Schenk, *Chem. Rev.*, 2006, **106**, 3338–3363.
- 9 D. A. Kopp and S. J. Lippard, *Curr. Opin. Chem. Biol.*, 2002, **6**, 568–576.
- 10 T. J. Kappock and J. P. Caradonna, *Chem. Rev.*, 1996, **96**, 2659–2756.
- 11 P. Nordlund and P. Reichard, *Annu. Rev. Biochem.*, 2006, **75**, 681–706.
- 12 P. J. Riggs-Gelasco, L. J. Shu, S. X. Chen, D. Burdi, B. H. Huynh, L. Que Jr. and J. Stubbe, *J. Am. Chem. Soc.*, 1998, **120**, 849–860.
- 13 S. K. Lee, B. G. Fox, W. A. Froland, J. D. Lipscomb and E. Münck, *J. Am. Chem. Soc.*, 1993, **115**, 6450–6451.
- 14 S. K. Lee, J. C. Nesheim and J. D. Lipscomb, *J. Biol. Chem.*, 1993, **268**, 21569–21577.
- 15 K. E. Liu, D. L. Wang, B. H. Huynh, D. E. Edmondson, A. Salifoglou and S. J. Lippard, *J. Am. Chem. Soc.*, 1994, **116**, 7465–7466.
- 16 K. E. Liu, A. M. Valentine, D. L. Wang, B. H. Huynh, D. E. Edmondson, A. Salifoglou and S. J. Lippard, *J. Am. Chem. Soc.*, 1995, **117**, 10174–10185.
- 17 F. C. Anson, J. A. Christie, T. J. Collins, R. J. Coots, T. T. Furutani, S. L. Gipson, J. T. Keech, T. E. Frafft, B. D. Santarsiero and G. H. Spies, *J. Am. Chem. Soc.*, 1984, **106**, 4460.
- 18 A. Stassinopoulos, G. Schulte, G. C. Papaefthymiou and J. P. Caradonna, *J. Am. Chem. Soc.*, 1991, **113**, 8686–8697.
- 19 S. Mukerjee, A. Stassinopoulos and J. P. Caradonna, *J. Am. Chem. Soc.*, 1997, **119**, 8097–8098.
- 20 G. T. Rowe, C. E. Rogge, E. V. Rybak-Akimova and J. P. Caradonna, *Chem.–Eur. J.*, 2008, **14**, 8303–8311.
- 21 G. T. Rowe, E. V. Rybak-Akimova and J. P. Caradonna, *Inorg. Chem.*, 2007, **46**, 10594–10606.
- 22 P. J. Cappillino, G. T. Rowe, P. C. Tarves, C. E. Rogge, A. M. Spuches, A. Stassinopoulos, W. Lo, W. H. Armstrong and J. P. Caradonna, *Inorg. Chim. Acta*, 2009, **262**, 2136–2150.
- 23 T. L. Foster and J. P. Caradonna, *J. Am. Chem. Soc.*, 2003, **125**, 3678–3679.
- 24 T. C. Bruice and W. A. Lee, *J. Am. Chem. Soc.*, 1985, **107**, 513–514.
- 25 T. C. Bruice and L. C. Yuan, *J. Am. Chem. Soc.*, 1985, **107**, 512–513.
- 26 R. D. Hancock, H. Maumela and A. S. de Sousa, *Coord. Chem. Rev.*, 1996, **148**, 315–347.
- 27 C.-C. Su, J. W. Reed and E. S. Gould, *Inorg. Chem.*, 1973, **12**, 337–342.
- 28 D. R. Pesiri, D. K. Morita, T. Walker and W. Tumas, *Organometallics*, 1999, **18**, 4916–4924.
- 29 J. Colby, D. I. Stirling and H. Dalton, *Biochemical Journal*, 1977, **165**, 395–402.
- 30 M. H. Sazinsky, J. Bard, A. Di Donato and S. J. Lippard, *J. Biol. Chem.*, 2004, **279**, 30600–30610.
- 31 D. A. Whittington, A. C. Rosenzweig, C. A. Frederick and S. J. Lippard, *Biochemistry*, 2001, **40**, 3467–3482.
- 32 P. F. Fitzpatrick, *Annu. Rev. Biochem.*, 1999, **68**, 355–381.
- 33 E. Solomon, I. T. C. Brunold, M. I. Davis, J. N. Kemsley, S.-K. Lee, N. Lehnert, F. Neese, A. J. Skulan, Y.-S. Yang and J. Zhou, *Chem. Rev.*, 2000, **100**, 235–349.
- 34 S. Spector, R. Gordon, A. Sjoerdsma and S. Udenfriend, *Molecular Pharmacology*, 1967, **3**, 549–555.
- 35 M. H. Sazinsky and S. J. Lippard, *J. Am. Chem. Soc.*, 2004, **127**, 5814–5825.
- 36 U. Hintermair, G. Francio and W. Leitner, *Chem. Commun.*, 2011, **47**, 3691–3701.